MODELING THE INFLUENCE OF FUEL INJECTION AND CHARGE AIR PARAMETERS ON THE EXHAUST EMISSIONS OF A MARINE DIESEL ENGINE

DO VAN DOAN*, NGUYEN VAN HAI

Faculty of Marine Engineering, Vietnam Maritime University

**Corresponding email: dovandoan@vimaru.edu.vn*

DOI: https://doi.org/10.65154/jmst.1065

Abstract

This study investigates the influence of operational parameters, specifically fuel injection characteristics and charge air conditions, on the combustion performance and exhaust gas composition (NOx, CO) of a four-stroke marine diesel engine. A comprehensive physical model, integrating a one-dimensional (1D) flow model for the gas exchange system and a three-dimensional (3D) combustion model within the cylinder, was developed and validated against experimental laboratory data. Simulation results indicate that variations in the fuel spray cone angle, along with charge air pressure and temperature, significantly impact the ignition delay, heat release rate, and emission concentrations. Specifically, an increase in charge air pressure prolongs the combustion process and reduces NOx formation, whereas elevated charge air temperatures increase NOx emissions up to a threshold of 75^0C. The study confirms that the proposed thermodynamic model is a reliable tool for optimizing the combustion process and controlling emissions in large marine engines, thereby reducing the need for costly empirical testing.

Keywords: *Marine diesel engine, combustion modeling, exhaust emissions, fuel injection, charge air parameters.*

1. Introduction

The global commercial fleet relies predominantly on internal combustion engines which, despite their high thermal efficiency, contribute significantly to anthropogenic air pollution. According to the International Maritime Organization (IMO), international shipping accounts for approximately 2.6% of global CO_2 emissions, alongside substantial quantities of highly toxic nitrogen oxides (NO_x) and carbon monoxide (CO) [1, 12, 13]. To mitigate these environmental impacts, the IMO has enforced stringent regulatory frameworks, notably MARPOL Annex VI. In Vietnam, recent domestic studies have focused on experimental maritime emission solutions, such as exhaust gas recirculation (EGR), to proactively control NO_x levels on operational vessels. These international mandates, including the Ship Energy Efficiency Management Plan (SEEMP) and the Energy Efficiency Operational Indicator (EEOI), make it a strict legal requirement for marine engineers to simultaneously maintain peak thermodynamic efficiency and control emission levels during vessel operation [2, 3, 4].

The formation mechanisms of NO_x - primarily governed by the thermal (Zeldovich) and prompt (Fenimore) pathways and CO are highly dependent on localized in-cylinder temperatures, pressures, and mixture homogeneity. While these kinetic mechanisms are well-documented, a significant limitation in the current literature is that the vast majority of existing combustion and diagnostic studies focus on small-scale, high-speed automotive engines. Marine diesel engines, however, possess fundamentally distinct design characteristics: massive cylinder displacements, low rotational speeds, extended strokes, and exceptionally high boost pressures [5, 6]. Consequently, the thermodynamic behaviors and emission trends in large-bore marine engines often directly contradict those observed in automotive applications. Directly extrapolating automotive combustion models or diagnostic parameters to marine engines is therefore scientifically inaccurate, creating a critical knowledge gap in marine-specific engineering literature [9].

In actual maritime operations, engine components inevitably degrade, leading to typical faults such as fuel injector fouling, altered injection spray patterns, or charge air cooler degradation. These malfunctions distort the optimized combustion process, causing a sudden surge in fuel consumption and toxic emissions. Recent domestic research has utilized numerical simulations to evaluate the correlation between fuel injection pressure and soot emission characteristics [10, 11]. However, traditional diagnostic methods,

TẠP CHÍ ISSN: 1859-316X, e-ISSN: 3093-3161
KHOA HỌC CÔNG NGHỆ HÀNG HẢI
JOURNAL OF MARINE SCIENCE AND TECHNOLOGY

which rely heavily on expensive in-cylinder pressure sensors or subjective intuition-based evaluations, are often prone to sensor failure in harsh environments or result in false evaluations. Recently, Artificial Neural Networks (ANN) have been proposed for automated fault detection; however, these methods require massive, high-fidelity datasets of engine faults to prevent overfitting. Gathering such extensive fault data solely through destructive physical testing on operational vessels is practically and economically impossible [7, 8].

To bridge this research gap, this study employs a multi-scale numerical approach, integrating a one-dimensional (1D) system simulation (AVL Boost) with a three-dimensional Computational Fluid Dynamics (3D CFD - AVL Fire) framework utilizing the 3Z-ECFM combustion model. Unlike previous studies that focus purely on general performance optimization, this research systematically isolates and quantifies the physical impact of varying specific fuel spray cone angles, boost air pressures, and boost air temperatures on the localized formation of NO_x and CO inside a large-bore marine engine. By establishing a rigorously validated numerical framework, this study generates a comprehensive, quantitative database of thermodynamic and emission "fault patterns". This foundational physical data addresses the critical missing link in current literature, providing the indispensable baseline required to train and develop future automated, emission-based diagnostic systems for smart vessels.

2. Research Methods and Models

To conduct a comprehensive investigation into the complex physical and chemical phenomena occurring within the engine, this study employs a multi-scale modeling approach, integrating one-dimensional (1D) thermodynamic simulation with three-dimensional Computational Fluid Dynamics (3D CFD). This integration leverages the computational efficiency of 1D system-level modeling to establish precise boundary conditions for the 3D simulation space within the cylinder.

2.1. Research Subject and 1D Simulation Setup

The reference subject for model development and validation is the AL25/30 turbocharged four-stroke Diesel engine manufactured by Cegielski-Sulzer. This is a representative medium-speed engine series, widely utilized as main propulsion engines or prime movers for generators on modern commercial vessels.

The gas exchange system (including the turbocharger, charge air cooler, and intake/exhaust manifolds) was programmed using the AVL Boost software platform. This 1D model solves the conservation equations for mass and energy along the piping length, enabling the assessment of pressure drops and mass flow rates under varying throttling characteristics. The pressure and temperature results at the intake/exhaust valves from the 1D model are extracted to serve as time-dependent boundary conditions for the 3D CFD model [7, 8].

Table 1. Fundamental technical specifications and operational parameters of the AL25/30 engine

Parameter	Value	Unit
Engine Basics		
Engine type	4-stroke, turbocharged	-
Rated power	250	kW
Rated rotational speed	750	rpm
Number of cylinders	3	-
Cylinder bore	250	mm
Piston stroke	300	mm
Compression ratio	12.7	-
Fuel Injection System		
Fuel injection timing	18	^{0}BTDC
Number of nozzle holes	9	-
Nozzle hole diameter	0.325	mm
Nominal injection opening pressure	25	MPa
Nominal fuel spray cone angle (φ)	144	degree
Gas Exchange & Turbocharging		
Turbocharger type	VTR 160 Brown-Boveri	-
Nominal charge air absolute pressure	182.69	kPa

2.2. Governing Equations in 3D CFD Space

In-cylinder fluid dynamics are simulated using the AVL Fire platform, which solves the Reynolds-Averaged Navier-Stokes (RANS) equations. The governing equations for mass and momentum conservation are expressed as follows:

Mass Conservation Equation (Continuity Equation):

$$\frac{\partial \rho}{\partial t} + \nabla \cdot (\rho \vec{u}) = S_m \quad (1)$$

Where ρ is the mixture density (kg/m^3), $\vec{u}$ is

the velocity vector of the gas phase (*m/s*), *t* is the time *(s)* and S_m is the mass source term resulting from the evaporation of the fuel spray ($kg/m^3.s$).

Momentum Conservation Equation:

$$\frac{\partial(\rho\vec{u})}{\partial t} + \nabla\cdot(\rho\vec{u}\vec{u}) = -\nabla p + \nabla\cdot\boldsymbol{\tau} + \rho\vec{g} + \vec{F}_s \quad (2)$$

In this equation, p denotes static pressure *(Pa)*, $\boldsymbol{\tau}$ represents the viscous stress tensor (N/m^2), $\vec{g}$ is the gravitational acceleration (m/s^2), and $\vec{F}_s$ is the momentum interaction force exerted by the fuel droplets (dispersed phase) on the gas phase (N/m^3).

The Standard $k-\epsilon$ turbulence model is deliberately employed in this study. For large-bore marine engines characterized by massive cylinder displacements and relatively low rotational speeds, the Standard $k-\epsilon$ model demonstrates superior robustness and stability in capturing large-scale eddy structures and strong swirl motions during the compression and injection strokes compared to other variants.

2.3. Fuel Spray and Combustion Kinetics Models

To simulate fuel atomization under high-pressure conditions, the Euler-Lagrange particle tracking method is employed. The aerodynamic droplet breakup is governed by the WAVE model, while the Dukowicz model calculates droplet heat transfer and evaporation. The droplet size distribution is evaluated using the Sauter Mean Diameter (SMD):

$$D_{32} = \frac{\sum_{i=1}^{n} N_i d_i^3}{\sum_{i=1}^{n} N_i d_i^2} \quad (3)$$

Where: n_i: Number of droplets in size class i, d_i: Diameter of droplets in size class i (m).

Regarding the combustion process, the 3-Zones Extended Coherent Flame Model (3Z-ECFM) is explicitly selected. This model is highly suitable for large-bore marine diesel engines because it effectively decouples complex chemical kinetics from turbulent mixing calculations. By partitioning the computational domain into unburned, mixed (flame), and burned zones, it accurately captures both the premixed and diffusion combustion phases. The mean fuel consumption rate $\overline{\omega}_F$ is determined based on the flame surface density Σ as follows:

$$\overline{\omega}_F = \rho_u Y_{F,u} S_L \Sigma \quad (4)$$

In this expression, $\bar{\omega}_F$: Mean fuel consumption rate ($kg/m^3.s$), ρ_u: Density of the unburned zone (kg/m^3), $Y_{F,u}$: Fuel mass fraction in the unburned zone, S_L: Laminar flame speed (*m/s*) and Σ: Flame surface density *(1/m)*.

2.4. Emission Models

Nitrogen oxide (NO_x) formation is calculated separately from the main combustion model to optimize computational resources, utilizing the Extended Zeldovich mechanism. This mechanism comprises three fundamental reversible chemical reactions that dominate NO formation at high temperatures (above 1800K):

$$O + N_2 \rightleftharpoons NO + N$$
$$O + N_2 \rightleftharpoons NO + N \quad (5)$$
$$ON + OH \rightleftharpoons NO + H$$

Where: [NO], [O], [N_2], [O_2], [OH]: Molar concentrations of the respective species (mol/m^3).

The total NO formation rate is calculated according to kinetic equations:

$$\frac{d[NO]}{dt} = 2k_1[O][N_2]\frac{1-\frac{[NO]^2}{K[O_2][N_2]}}{1+\frac{k_{-1}[NO]}{k_2[O_2]+k_3[OH]}} \quad (6)$$

Where: k_1, k_2, k_3: Forward reaction rate constants for the three reactions in Eq.5 *(m^3/mol.s)*, k_{-1}: Reverse reaction rate constant for the first reaction in Eq.5 *(m^3/mol.s)*, *K:* Equilibrium constant.

Additionally, the Fenimore model is activated to account for prompt NO_x formation in flame regions with high hydrocarbon (CH) radical concentrations. The formation and oxidation of Carbon Monoxide (CO) are simulated through a detailed chemical kinetic network that governs the dissociation balance of CO, CO_2, O, and OH radicals at the end of the expansion stroke.

2.5. Mesh Generation and Computational Scenarios

To simulate in-cylinder volume changes, a hexahedral moving mesh is utilized. A rigorous mesh independence study was conducted evaluating three configurations: Mesh A (full 3D cylinder including moving valves) and Meshes B & C (simplified 1/9 symmetrical sectors). While sector meshes reduced computational time, Mesh A was explicitly selected to accurately capture the asymmetric gas exchange processes and the complete turbulent flow field. The structure of the moving mesh inside the combustion chamber at top dead center (TDC) is described in Figure 1.

To balance computational cost and convergence accuracy, the grid was locally refined to 1-2 mm within the fuel injection and combustion regions, and down to 0.125mm near the valve seats. The optimized Mesh A comprises approximately 500,000 cells at Top

TẠP CHÍ ISSN: 1859-316X, e-ISSN: 3093-3161
KHOA HỌC CÔNG NGHỆ HÀNG HẢI
JOURNAL OF MARINE SCIENCE AND TECHNOLOGY

Dead Center (TDC), dynamically expanding to 1.5 million cells during the gas exchange phase. The SIMPLE algorithm is applied to resolve the pressure-velocity coupling, utilizing an adaptive time-step that ranges from 1°CA during the compression stroke down to 0.02°CA during injection and combustion, ensuring optimal numerical stability and high-resolution accuracy.

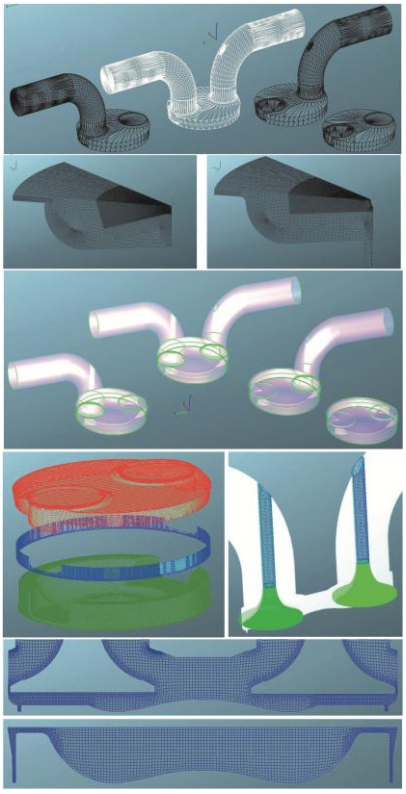

Figure 1. Structure of the dynamic moving mesh inside the combustion chamber at TDC

2.6. Model Validation

The reliability of the proposed 3D CFD model is validated against experimental data acquired from the AL25/30 engine test bench. As illustrated in Figures 2 and 3, the simulated in-cylinder pressure curves demonstrate excellent quantitative agreement with the experimental data, yielding a mean relative error of only 1.42% for the peak indicated pressure. Furthermore, the deviations for NO_x and O_2 concentrations are remarkably low, recorded at 1.2% and 0.4%, respectively.

However, it is scientifically imperative to acknowledge the limitations of the current RANS-based CFD framework regarding carbon-based emissions. While the model accurately captures the qualitative trends of Carbon Monoxide (CO) and Carbon Dioxide (CO_2) under varying loads and fault conditions, it cannot achieve precise quantitative validation. This discrepancy stems from the extreme complexity of localized incomplete combustion, fuel wall-impingement, and cold-wall quenching near the low-temperature cylinder boundaries, which are micro-scale kinetic phenomena not fully resolved by macroscopic RANS turbulence models. Consequently, the CO emission results presented in this study are strictly utilized for qualitative trend analysis rather than absolute quantitative predictions.

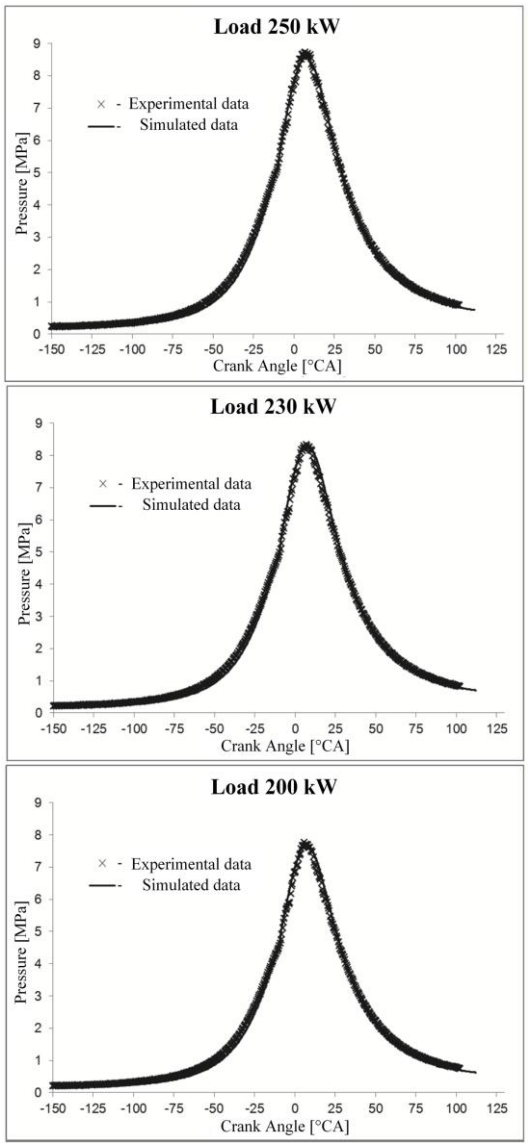

Figure 2. Comparison of indicated pressure versus crank angle between experimental and simulated data P-α diagram

3. Results and Discussion

Following the successful model validation, with

the peak indicated pressure error at 1.42% and the NO_x deviation at 1.2% compared to experimental data, independent parametric investigations were conducted for each variable.

3.1. Influence of Fuel Spray Cone Angle (φ)

The investigation into the fuel spray cone angle (φ) was specifically conducted at the engine's maximum continuous rating (100% load, 250kW). The scientific rationale for selecting this maximum load is that the injected fuel mass and spray momentum possess the highest kinetic energy. Under these extreme conditions, physical phenomena related to spray distribution, turbulent mixing, and potential wall-impingement on the cylinder boundaries are most pronounced and observable. Simulations were performed using a nominal angle of 144°, alongside extended boundary values of 132°, 138°, 150°, and 156°.

Varying the spray cone angle did not significantly alter the initial auto-ignition timing or the fuel vapor

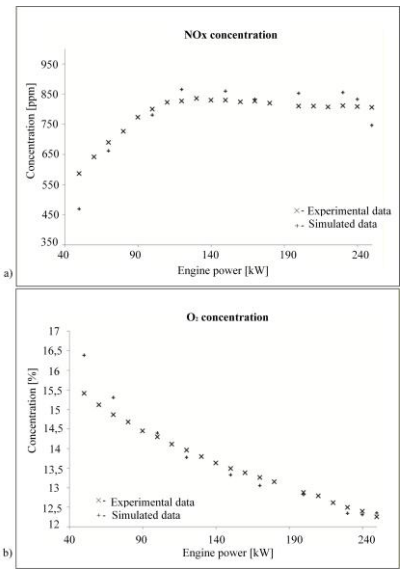

Figure 3. Comparison of NOx and O_2 percentages in exhaust gas between simulation calculations and experimental measurements.

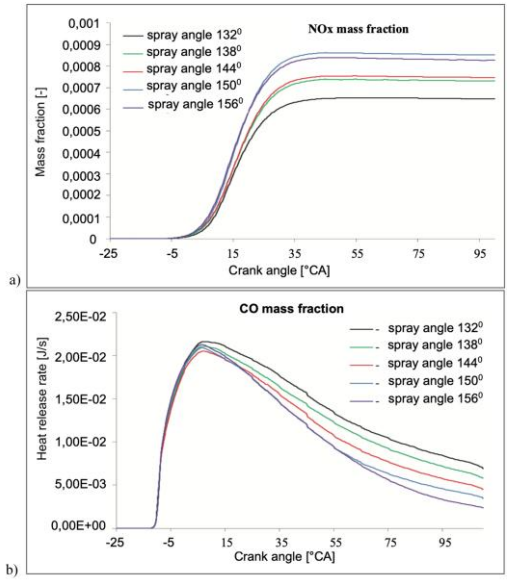

Figure 4. Influence of fuel spray cone angle on in-cylinder concentration of: a) NOx and b) CO

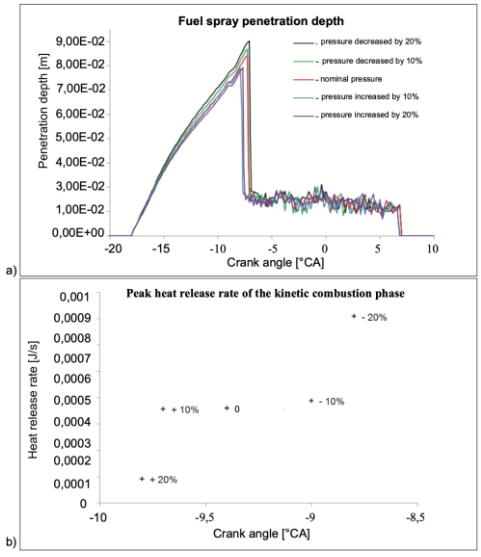

Figure 5. Influence of boost pressure on combustion parameters: a) fuel spray penetration depth, b) location of peak burning rate

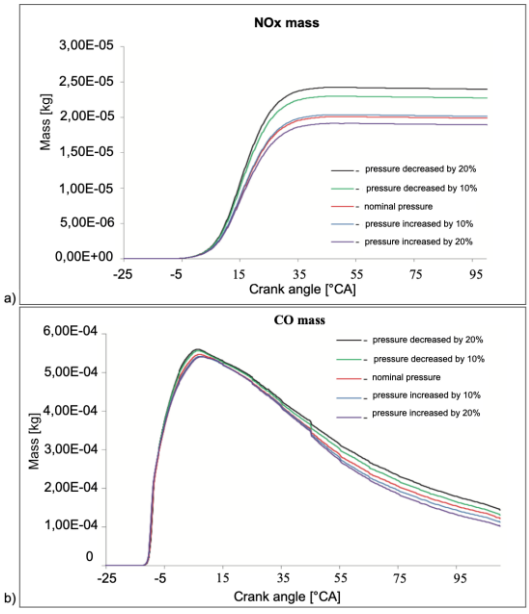

Figure 6. Influence of boost pressure on in-cylinder mass of: a) NOx and b) CO

TẠP CHÍ ISSN: 1859-316X, e-ISSN: 3093-3161
KHOA HỌC CÔNG NGHỆ HÀNG HẢI
JOURNAL OF MARINE SCIENCE AND TECHNOLOGY

mass flow rate. However, increasing the spray angle noticeably shifted the combustion kinetics. A wider angle prolongs the kinetic (premixed) combustion phase while shortening the diffusion phase, resulting in an overall acceleration of the combustion process. Consequently, peak in-cylinder pressure and temperature increased significantly. Spatial visualizations of the flow field confirm that an optimized spray distribution accelerates the oxidation of local fuel-rich zones, thereby minimizing incomplete combustion and effectively reducing the Carbon Monoxide (CO) residual mass fraction (Figure 4b).

From an ecological perspective, the elevated peak temperatures and pressures associated with wider spray angles strongly stimulate the Zeldovich thermal mechanism, leading to a proportional increase in NO_x formation (Figure 4a). Notably, at the extreme angle of 156°, the expanded spray momentum directly impacts the cylinder head and liner. This physical wall-impingement induces a localized cold-wall quenching effect, which causes thermal losses and partially suppresses the global peak temperature. As a result, the NO_x formation trend slightly reverses, yielding lower NO_x levels compared to the 150° configuration.

3.2. Influence of Boost Air Pressure

Faults in the gas exchange system (e.g., intake fouling) directly alter the pressure and mass of air supplied to the cylinder. Simulations were conducted with initial pressure fluctuations from -20% to +20% relative to nominal values (Table 2). Increased boost pressure leads to higher charge density at the end of compression, which reduces fuel injection velocity and spray penetration depth.

Table 2. Simulated scenarios of initial charge air pressure variations

Condition	Absolute pressure	Unit
-20%	166.15	kPa
-10%	174.42	kPa
Nominal (0%)	182.69	kPa
+10%	190.96	kPa
+20%	199.23	kPa

Increased boost pressure enhances the air density at the end of compression. The aerodynamic drag slows the injection velocity and reduces the fuel spray penetration depth (Figure 5a). Due to shifts in droplet size distribution, the intensity of the kinetic combustion phase is visibly suppressed, causing auto-ignition to occur slightly earlier (0.2°CA) while the overall combustion process is prolonged.

Due to the prolonged, smoother combustion combined with a constant air mass acting as a "heat sink," the peak combustion temperature decreases. According to Figure 6, this directly inhibits the nitrogen oxidation process, significantly reducing NOx formation. Abundant air also promotes the oxidation of carbon residuals, leading to a decrease in CO levels.

3.3. Influence of Boost Air Temperature

Simulations representing charge air cooler efficiency degradation were deliberately performed at the engine's minimum operational load. The scientific rationale for this selection is that at minimum load, the injected fuel mass is extremely small, creating a globally lean mixture with an exceptionally high excess air ratio. Under these boundary conditions, the combustion kinetics become highly sensitive to thermodynamic fluctuations in the intake air, making it the optimal operating point to evaluate emission deviations. Initial charge air temperatures were parametrically varied from 70°C to 80°C.

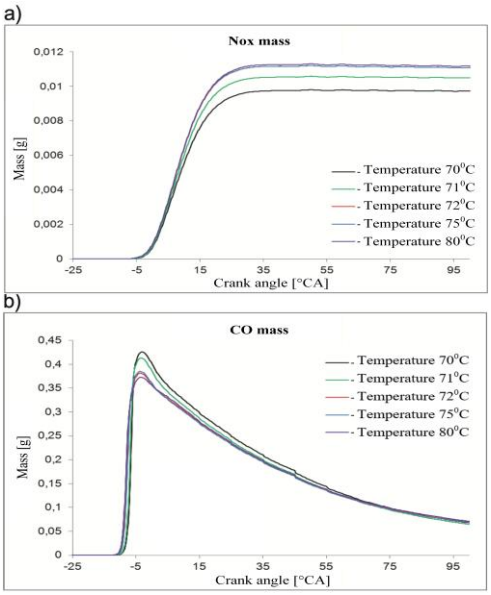

Figure 7. Influence of boost air temperature on gas mixture concentration of: a) NOx and b) CO

Elevated intake temperatures significantly shorten the ignition delay and advance the initial kinetic combustion phase. This thermodynamic shift results in a substantial surge in local peak combustion temperatures (an increase of approximately 28°C), whereas the peak in-cylinder pressure experiences a negligible reduction of 1%. From an ecological perspective, the escalated peak temperatures strongly promote the Zeldovich thermal mechanism, leading to

a proportional increase in NO_x emissions. However, a distinct saturation point is observed when the intake air temperature exceeds 75°C.

This saturation stems from accelerated fuel evaporation creating localized oxygen-deficient zones, which kinetically inhibit further nitrogen oxidation (Figure 7a). Conversely, while elevated temperatures initially suppress CO formation, final concentrations at Exhaust Valve Open (EVO) paradoxically increase. This behavior is governed by high-temperature dissociation kinetics during the late expansion phase, preventing complete secondary oxidation of carbon residuals (Figure 7b).

4. Conclusion

This study employed a validated 1D-3D CFD model (AVL Boost/Fire, 3Z-ECFM) to quantify operational impacts on marine diesel emissions. Key findings include: (1) Widening fuel spray angles accelerates kinetic combustion, elevating NO_x levels; however, extreme angles ($> 150^0$) induce spray impingement and local thermal losses, reversing this trend. (2) Increased boost air pressure acts as a gas-dynamic buffer, extending combustion duration and mitigating peak temperatures, thereby reducing both NO_x and CO emissions. (3) Elevated intake temperatures advance the combustion phase, causing NO_x to surge before reaching saturation beyond 75^0C. These quantitative insights establish a robust physical data matrix essential for optimizing ecological performance and informing future condition-based monitoring and fault diagnostic strategies.

Acknowledgements

This research is funded by Vietnam Maritime University under grant number: **DT25-26.31**.

REFERENCES

[1] International Maritime Organization (2020), *Reduction of GHG emissions from ships - Fourth IMO GHG Study 2020 - Final Report*, London: IMO Publishing.

[2] Zeldovich, Y. B. (1946), *The oxidation of nitrogen in combustion explosions*, Acta Physicochimica U.S.S.R., Vol.21, pp.577-628.

[3] Lavoie, G. A., Heywood, J. B., & Keck, J. C. (1970), *Experimental and theoretical study of nitric oxide formation in internal combustion engines,* Combustion Science and Technology, pp.313-326.

[4] Fenimore, C. P. (1971), *Formation of nitric oxide in premixed hydrocarbon flames, 13th Symposium (International) on Combustion*, Vol.13, pp.373-380.

[5] Colin, O., & Benkenida, A. (2004), *The 3-Zones extended coherent flame model (ECFM3Z) for computing premixed/diffusion combustion*, Oil & Gas Science and Technology, Vol.59(6), pp.593-609.

[6] Sarvi, A., Fogelholm, C. J., & Zevenhoven, R. (2008), *Emissions from large-scale medium-speed diesel engines: 1. Influence of engine operation mode and turbocharger*, Fuel Processing Technology, Vol.89, pp.510-519.

[7] AVL List GmbH (2014), *AVL FIRE Combustion Module Manual*, Gratz, Austria: AVL List GmbH.

[8] Mobasheri, R., & Peng, Z. (2013), *CFD investigation into diesel fuel injection schemes with aid of homogeneity factor*, Computers & Fluids, Vol.77, pp.12-23.

[9] Kowalski, J. (2014), *An experimental study of emission and combustion characteristics of marine diesel engine with fuel pump malfunctions*, Applied Thermal Engineering, Vol.65, pp.469-479.

[10] Tran The Nam (2022), *Experimental study on exhaust gas recirculation solutions for reducing NOx emissions from in-service marine diesel engines*, Journal of Marine Science and Technology, Vol.64, pp.14-18.

[11] Mai Duc Nghia & Ho Duc Tuan (2024), *Simulation of the correlation between soot emissions and fuel injection pressure in fishing vessel diesel engines*, Journal of Fisheries Science and Technology, Vol.4(2023).

[12] Pham Van Viet & Do Van Doan (2025), *Assessment of emission characteristics of a diesel engine fueled with biodiesel combined with hydrogen induction in the intake manifold using numerical simulation*, Journal of Marine Science and Technology, Vol.83, pp.93-98.

[13] Do Van Doan & Nguyen Thi Hong Nhung (2026), *Effects of adding nano graphite oxide additives to ULSD-biodiesel blends on the performance and emission characteristics of a marine diesel engine,* Journal of Chemistry and Application, Vol.01(78), pp.58-63.

Received:	08/03/2026
Revised:	04/04/2026
Accepted:	10/04/2026